Available online at www.sciencedirect.com
ScienceDirect
Journal of Sound and Vibration 321 (2009) 837–853
JOURNAL OF SOUND AND VIBRATION
www.elsevier.com/locate/jsvi

Finite element investigation of traffic induced vibrations

Shen-Haw Ju*

Department of Civil Engineering, National Cheng-Kung University, Tainan 70101, Taiwan, ROC

Received 25 October 2007; received in revised form 9 October 2008; accepted 25 October 2008
Handling Editor: J. Lam
Available online 23 December 2008

Abstract

This paper investigates the characteristics of building vibrations induced by adjacent moving trucks using finite element analyses. A finite element is developed to simulate complicated vehicles, and theoretical as well as experimental methods are used to validate it. The parametric study indicates that road irregularity is the major cause of truck vibrations around their vertical natural frequencies. If the natural frequencies of the truck approach the building's natural frequencies, resonance occurs, and building vibrations increase. To reduce building vibrations generated by moving trucks, road roughness should be as small as possible. A simpler method to reduce truck vibrations is to slow down the truck. Moreover, the coincidence of the building's first natural frequency and the truck's vertical natural frequency should be avoided.

1. Introduction

Ground vibrations induced by road traffic are a major environmental issue, especially for near-by hospitals and high-tech industries, since such vibrations may affect surgery or high-tech production. Moreover, large vibrations are uncomfortable for people. Thus, predicting the response of buildings induced by road traffic vibration is becoming increasingly important. Hunaidi and Tremblay [1] performed measurements and analyses of building vibration induced by road traffic, and the levels were evaluated with reference to human annoyance and the potential for building damage using existing standards. Maeda et al. [2] recorded road traffic-induced building vibrations continuously for 24 h, both outside and inside a building. Several alternative objective methods of quantifying the severity of exposure to whole-body road traffic-induced building vibration were used. Clemente and Rinaldis [3] analyzed the traffic-induced vibrations in the basement of a building. Wave propagation in the soil around the building in the presence of anti-vibration paving was compared with that in the absence of such paving. Hao and Ang [4] presented an analytical method to estimate the power spectral densities of traffic-induced ground vibrations, which are assumed to consist of primarily Rayleigh waves induced by moving forces that propagate along the surface of an elastic homogeneous half-space. Hao et al. [5] presented traffic-induced ground vibrations measured at four soil sites. Their characteristics in terms of the site conditions and distance to road center were discussed. Lombaert et al. [6] made a numerical model of free field traffic-induced vibrations during the passage of a vehicle on an uneven

*Tel.: +886 6 2757575x63119; fax: +886 6 2358542.
E-mail address: juju@mail.ncku.edu.tw

0022-460X/$ - see front matter © 2008 Elsevier Ltd. All rights reserved.
doi:10.1016/j.jsv.2008.10.031

road, which subjected the vehicle to vertical oscillations that cause dynamic axle loads and vibrations. Hunaidi et al. [7] investigated the effect of bus suspension systems on building vibrations with the results showing that the dynamic component of pavement loads induced by the two buses were significantly different, but the difference in building vibration levels was not as significant. Lombaert and Degrande [8] validated a numerical model for the prediction of traffic-induced vibrations using experiments, in which the vibrations in the free field, generated by the passage of a vehicle on an uneven road, were predicted. Crispino and D'apuzzo [9] described the measurements of road traffic-induced vibrations in a building, which they then related to vehicle type and speed and compared with values obtained by a modified prediction model. Lombaert et al. [10] studied the influence of soil stratification on the free field vibrations generated by the passage of a vehicle on an uneven road. A two-stage solution procedure was applied for the numerical prediction of the free field traffic-induced vibrations. Clouteau et al. [11] computed free field vibrations induced by train or road traffic, in which the excitation was either deterministic or stochastic. Schevenels et al. [12] described the influence of seasonal variations of the groundwater table on free field traffic-induced vibrations. The passage of a truck on two types of road unevenness was considered. Pyl et al. [13] focused on the coupling of a validated source model for free field traffic-induced vibrations to a receiver model that enables one to predict the response of buildings. Xu and Hong [14] presented a framework for quantifying traffic-induced building vibration in a stochastic way with the results showing that traffic-induced ground vibration impedes the normal operations of a high-tech facility.

In the literature, the time-domain finite element method is not often used to simulate building vibrations induced by road traffic. Moreover, the characteristics of vehicle-induced vibrations for buildings are seldom clearly discussed. In this paper, a three-dimensional (3D) vehicle element is developed, and the time-domain finite element analyses are performed to investigate the behavior of the vehicle-induced building vibration. The major advantage of this method is that the numerical procedure is exactly the same as the traditional finite element analysis. In addition, the effects and relationships among road irregularities, truck speeds, truck natural frequencies and building natural frequencies were all investigated in this study.

2. 3D vehicle finite element formulation

Vehicles contain car bodies, bogies, wheel-axis sets, springs, and dampers, which are modeled as the combination of moving wheel elements, spring-damper elements, lumped masses and rigid links. The vehicle is assumed to move in the X direction (road direction), the vertical direction is in the Z direction, and the Y direction is perpendicular to the road.

2.1. Moving wheel element

The contact behavior between the road and wheel is modeled by a stiffness k_r, whose direction can be in the global X (road direction), Y, or Z direction. Ju et al. [15] developed a wheel element on the targets of two-node beam elements to solve the problem of trains moving on rails. In this study, vehicle wheels directly contact a road that is modeled by 3D 8-20-node isoparametric elements, so the target surface is the four to eight variable-number-node surface, as shown in Fig. 1. Stiffness k_r can be set to the average stiffness of the contact layer or a large value to ignore the contact behavior. A major disadvantage of this element is that the contact location is only a point, so the displacement at this contact point will increase when the element size decreases.

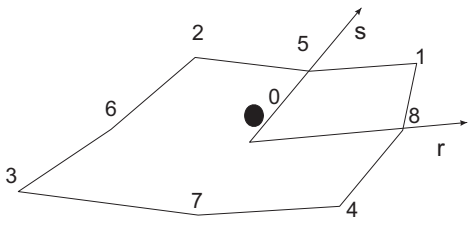

Fig. 1. Moving wheel element with a four to eight variable-number-nodes surface.

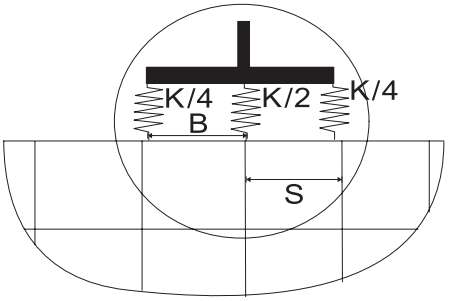

Fig. 2. Modeling a wheel contact region using several moving wheel elements with appropriate spring constants and element spaces ($B \cong S$, where B = spring space and S = soil element size).

To overcome this problem, nonlinear contact analysis should be performed. However, it is extremely difficult to model the road irregularity and wheel geometry well. An alternative is to model a wheel using several moving wheel elements with appropriate spring constants and element spaces, and the smallest soil element size is larger than or similar to the average space of the spring elements. An example is shown in Fig. 2, in which a wheel is modeled by three elements with the spring element space similar to that of the soil element. It should be noted that more elements for a wheel will obtain more realistic results, but will require more CPU time. The element stiffness in one of the X, Y, or Z direction is:

$$[S] = [T]^{\mathrm{T}}[T]k_r \tag{1}$$

where $[T] = [1 \ -N_1 \ -N_2 \ -N_3 \ -N_4 \ -N_5 \ -N_6 \ -N_7 \ -N_8]$ and N_1–N_8 are the interpolation functions of four to eight variable-number-node two-dimensional isoparametric element [16]. The equilibrium vehicle load F in the Z (vertical) direction should be transformed into nodes 1–8 to obtain the force vector $\{f\}$, as follows:

$$\{f\} = [N_1 \ N_2 \ N_3 \ N_4 \ N_5 \ N_6 \ N_7 \ N_8]^{\mathrm{T}}F \tag{2}$$

Wheel elements with a damper or mass will produce an unsymmetrical stiffness matrix, because the velocity field of node 2 requires the derivation of shape functions. To overcome this problem, only the stiffness was used in this study. Consequently, the spring-damping and lumped mass elements discussed in the next section can be connected to this element directly. To evaluate the irregularity between the road and wheel, the element forces $\{f_r\}$ of Eq. (3) must be added to the global force vector.

$$\{f_r\} = [T]^{\mathrm{T}}k_r r(X) \tag{3}$$

where $r(X)$ is a function of the road or rail irregularity that will be further discussed in Sections 3.1 and 4.3, and X is the wheel location in the moving wheel direction (X axis).

One could omit the interaction between the vehicle and the road, as the road is much stiffer than the vehicle. Thus, the dynamic loads could also have been calculated by considering the truck passing on a rigid, uneven road, which significantly simplifies the analysis, and gives a correct result in the case of road traffic. However, if one wants to know the ground vibration induced by the road traffic, the interaction between the vehicle and the road is still necessary.

2.2. Spring-damper, lumped mass and rigid link

The spring-damper element contains stiffness k_v and damping c_v in the X, Y, or Z direction. The stiffness or damping matrix of this element is

$$[S] = \begin{bmatrix} s & -s \\ -s & s \end{bmatrix} \tag{4}$$

For the damping matrix $s = c_v$, and for stiffness matrix $s = k_v$. $[S]$ can be directly added to the global stiffness or damping matrix. The lumped mass matrix of a rigid body at its gravity center is a standard diagonal matrix,

as follows:

$$[S] = [\backslash \ m \ m \ m \ I_x \ I_y \ I_z \ \backslash] \tag{5}$$

where m is the mass, and I_x, I_y, and I_z are the moments of inertia in three global directions, respectively.

Rigid links connect the above finite elements with rigid bodies. For small deformation in a rigid body, if the force F_i^S is known in the global i direction ($i = X$, Y or Z) at a slave node, the force and moments at the mass center, called the master node, can be calculated as follows:

$$F_i^M = F_i^S \tag{6}$$

$$\begin{Bmatrix} M_Y^M \\ M_Z^M \end{Bmatrix} = \begin{bmatrix} -\Delta Z \\ \Delta Y \end{bmatrix} F_X^S, \quad \begin{Bmatrix} M_X^M \\ M_Z^M \end{Bmatrix} = \begin{bmatrix} \Delta Z \\ -\Delta X \end{bmatrix} F_Y^S \quad \text{and} \quad \begin{Bmatrix} M_X^M \\ M_Y^M \end{Bmatrix} = \begin{bmatrix} -\Delta Y \\ \Delta X \end{bmatrix} F_Z^S \tag{7}$$

or

$$\{M^M\} = \{D\}F_i^S = \begin{Bmatrix} D_1 \\ D_2 \end{Bmatrix} F_i^S \tag{8}$$

where $(\Delta X, \Delta Y, \Delta Z)$ is the coordinate difference between the master and slave nodes, and $M_X^M, M_Y^M,$ and M_Z^M are the master-node moments in the X, Y, and Z directions, respectively.

For an n-degree-of-freedom mass, the damping or stiffness matrix ($[S^S]$) and the force vector ($\{F^S\}$) with a slave degree of freedom, $[S^M]$ and $\{F^M\}$, respectively, at the master node are:

$$[S^M] = \begin{bmatrix} & [I] & \\ [0]_1 & [D] & [0]_2 \end{bmatrix} [S^S] \begin{bmatrix} & [I] & \\ [0]_1 & [D] & [0]_2 \end{bmatrix}^T \quad \text{or} \quad [S^M] = [T][S^S][T]^T \tag{9}$$

$$\{F^M\} = [T]\{F^S\} \tag{10}$$

where $[I]$ is the n by n unit matrix, $[0]_1$ and $[0]_2$ are zero matrices, and $[D]$ is obtained from Eq. (8). For a one-dimensional spring or damper, whose two sides, L and R, are connected to two master nodes, and the direction of side L to R is the positive global X, Y, or Z direction, the stiffness or damping matrix can be calculated as follows, using Eqs. (4) and (9).

$$[S] = s\{B\}\{B\}^T \tag{11}$$

where $\{B\}^T = [1 \ \ -1 \ \ D_1^R \ \ D_2^R \ \ -D_1^L \ \ -D_2^L]$, D_1^R, D_2^R, D_1^L, and D_2^L are the D_1 and D_2 of Eq. (8) at sides R and L, respectively. If there is no connection with a master node at side R or L, the two terms of that side can be removed from vector $\{B\}$ or just set to zero.

2.3. Finite element model and validation

We assume that all the displacements, velocities, and accelerations at vehicle nodes in the motion (X) direction are relative to the current averaged displacement, velocity, and acceleration of the vehicle, respectively. The stiffness and damping forces of vehicles are independent of the average vehicle displacement and velocity, so the unknown terms change to the relative displacement and velocity. The mass forces due to the average vehicle acceleration in the motion direction can be calculated explicitly as inertia forces (masses multiplied by average vehicle acceleration). Thus, all the mass locations at vehicles are subjected to inertia forces in the negative acceleration direction [17]. After the above procedure, vehicle stiffness matrices are added to the finite element model with 3D solid or beam elements producing a linear small-displacement finite element analysis, and the moving train dynamic analysis with large dof can be found in the references [18,19].

In Fig. 3, the two-axle vehicle moving on a simply supported beam was analyzed to validate this finite element model, where the vehicle has four dof moving with a uniform speed of 30 m/s on a simply supported bridge 25 m long. The input data are: the cross section of the beam is a square shape with a size of 1 m, the mass per unit length is 1E4 kg/m, and Young's modulus is 2E11 N/m^2. The vehicle data shown in Fig. 3 are

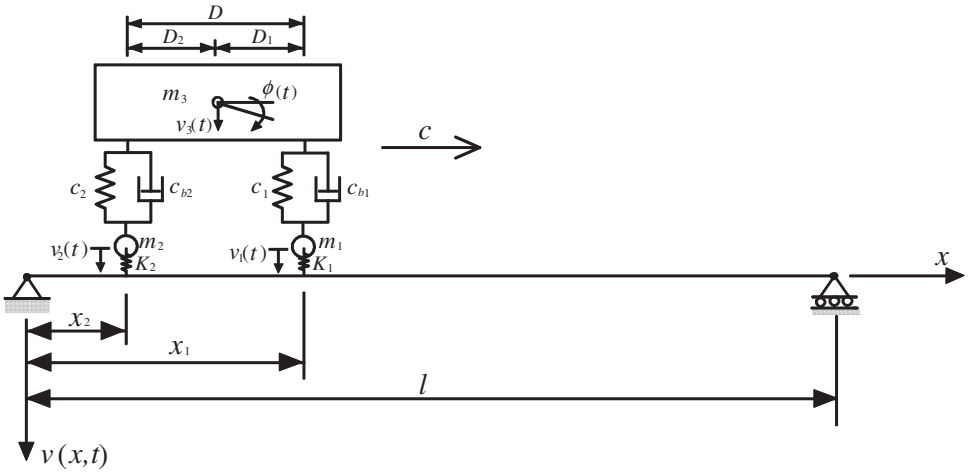

Fig. 3. A two-axle vehicle moving on a simply supported beam.

Table 1
Input parameters of the bridge and vehicle from Section 3 and Fig. 3.

Parameter	Description	Value
m_3	Mass of sprung part of vehicle	18E3 kg
m_1, m_2	Mass of unsprung part of vehicle	1E3 kg
K_1, K_2	Spring constant of ties	2E10 N/m
C_1, C_2	Spring constants for the two axles	8E6 N/m
P_1, P_2	Weight of unsprung part of vehicle	9.8E4 N
I	Mass moment of vehicle inertia	1E5 m^4
D	Vehicle axle base	14 m
D_1, D_2	Horizontal distance between the centroid of sprung mass and unsprung mass	7 m
C_{b1}, C_{b2}	Viscous damping for the two axles	2E4 N s/m

listed in Table 1. Fryba [20] generated the theoretical equations for this problem, which can be solved numerically using Newmark's method.

For finite element solutions, the vehicle is modeled by two wheel elements, two spring-damper elements, and a lumped mass. The master node is located at the center of the lumped mass, and the upper nodes of the two spring-damper elements are slaved nodes controlled by this master node. Three finite element meshes were generated to model the simply supported beam. Case 1 is the regular mesh (Fig. 4a) with 20-node isoparametric elements, case 2 is the irregular mesh (Fig. 4b) with 20-node isoparametric elements, and case 3 is the regular mesh (Fig. 4a) with 8-node incompatible isoparametric elements. Newmark's method and a consistent mass scheme were used to solve this problem with the two Newmark constants and time step lengths of 0.25, 0.5, and 0.002 s. The road roughness in the vertical directions was modeled by the following equation.

$$r(X) = \frac{a_r}{2}\sin(2\pi X/L_r) \tag{12}$$

where a_r is the amplitude of the road irregularity and L_r is the wavelength of the road irregularity. This study set $a_r = 0.01$ m and $L_r = 3$ m.

Fig. 5 shows a comparison of the displacements on beam and mass centers using Fryba's [20] and finite element solutions. Since the dashed and solid lines overlap, this figure indicates that the two solutions are almost identical. Moreover, regular, irregular, high-order, and incompatible meshes produce similar finite element results.

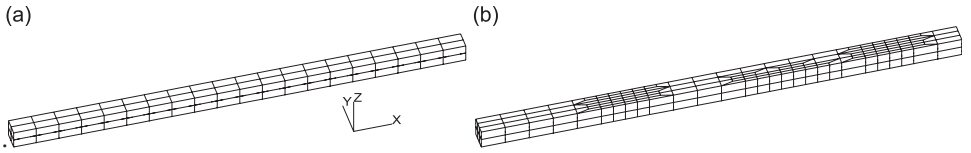

Fig. 4. Finite element meshes of the simple beam in Fig. 3: (a) regular mesh and (b) irregular mesh

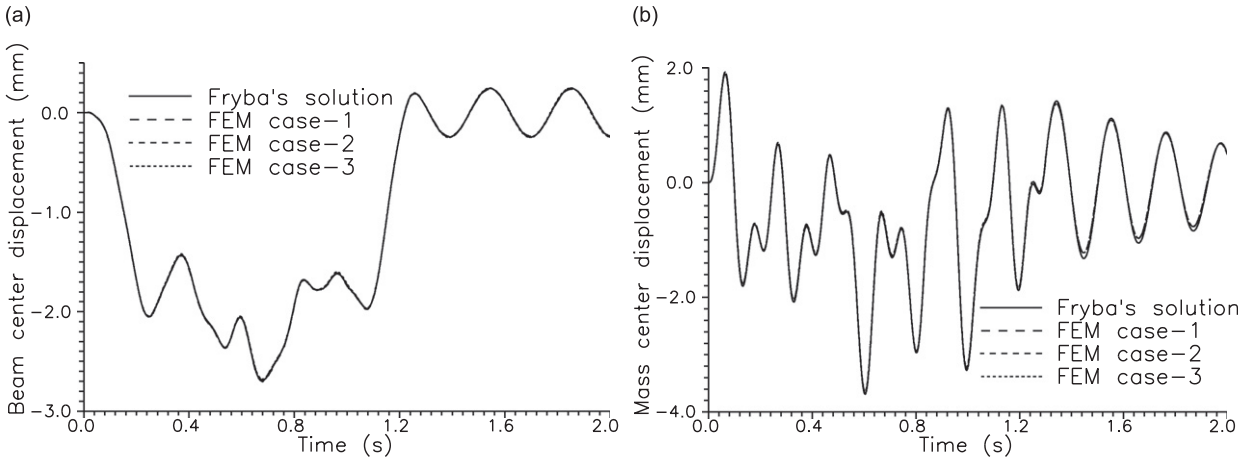

Fig. 5. Comparison of Fryba's [20] and finite element solutions for a two-axis vehicle passing a simply supported beam with road roughness: (a) beam center displacement and (b) master center displacement.

3. Investigating traffic induced vibrations using finite element analyses

3.1. Illustration of vehicle, road, soil, and building

The vehicle adopted in this study is a 35.9-T truck, whose dimensions, damping, and mass are shown in Fig. 6. The damping and stiffness values were obtained from the truck company, and a static loading test was used to validate the vertical stiffness values that are the most sensitive parameters for the truck vertical frequencies. A large stiffness of 1E6 kN/m was used between the road and wheel, which means that the stiffness is only used as a penalty constant and the flexibility of road and wheel contact is ignored. The first and second vertical natural frequencies of the truck are 2.6 and 3.3 Hz, respectively. In the finite element model, each wheel set of the truck is modeled by three spring-damper elements in the X, Y, and Z directions, the connection between the car head and truck is also modeled by three spring-damper elements in the X, Y, and Z directions, and the car bodies are modeled by two rigid bodies with a lumped mass at each mass center. The road has two lanes, for a total width of 7 m (3.5 m each lane), and a 30 cm thick asphalt layer with Young's modulus of 10 Gpa, Poisson's ratio of 0.25, and mass density of 2.0 T/m^3. The road irregularity is modeled using the following equation [21]:

$$r(X) = \sum_{k=1}^{N} a_k \cos(2\pi f_k X + \phi_k) \tag{13}$$

where a_k (m) is the amplitude of the cosine wave, f_k (cycles/m) is a frequency within the interval $[f_1,f_u]$ (cycles/m) in which the power spectral density function is defined, ϕ_k is a random phase angle with uniform probability distribution in the interval $[0,2\pi]$, X (m) is the global coordinate measured from the original point, and N is the total number of terms used to build up the road irregularities. The parameters a_k and f_k are

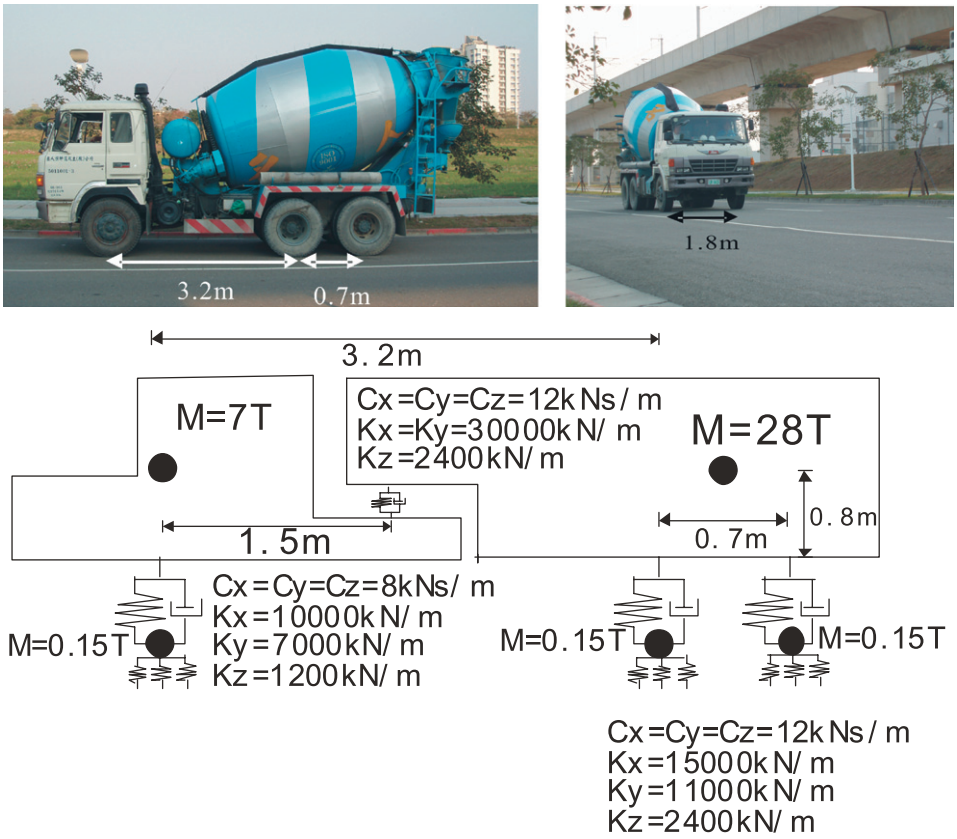

Fig. 6. The dimensions and mass of the adopted truck (total mass = 35.9 T, six wheels each with a spring-damper and a mass of 0.12 T).

Table 2
Road surface classification.

Road surface condition	A (m^2/(m/cycle))
Very good	$A \leqslant 0.24\times10^{-6}$
Good	$0.24\times10^{-6} < A \leqslant 1\times10^{-6}$
Average	$1\times10^{-6} < A \leqslant 4\times10^{-6}$
Poor	$4\times10^{-6} < A \leqslant 16\times10^{-6}$
Very poor	$16\times10^{-6} < A$

computed, respectively, using [22,23]

$$a_k = \sqrt{4G_r(f_k)\Delta f}, \quad k = 1,2,\ldots,N \tag{14}$$

$$f_k = f_l + (k-1/2)\Delta f, \quad k = 1,2,\ldots,N \tag{15}$$

$$\Delta f = (f_u - f_l)/N \tag{16}$$

$$G_r(f) = Af^{-\beta} \quad \text{for } f > 0.05 \text{ cycles/m} \quad \text{and} \quad G_r(f) = A(0.05)^{-\beta} \quad \text{for } f \leqslant 0.05 \text{ cycles/m} \tag{17}$$

where $G_r(f)$ (m^3/cycle) is the power spectral density function, A (m^3/cycle) is the spectral roughness coefficient as shown in Table 2, the exponent β is 2 (based on the international organization for standardization (ISO)), f_u

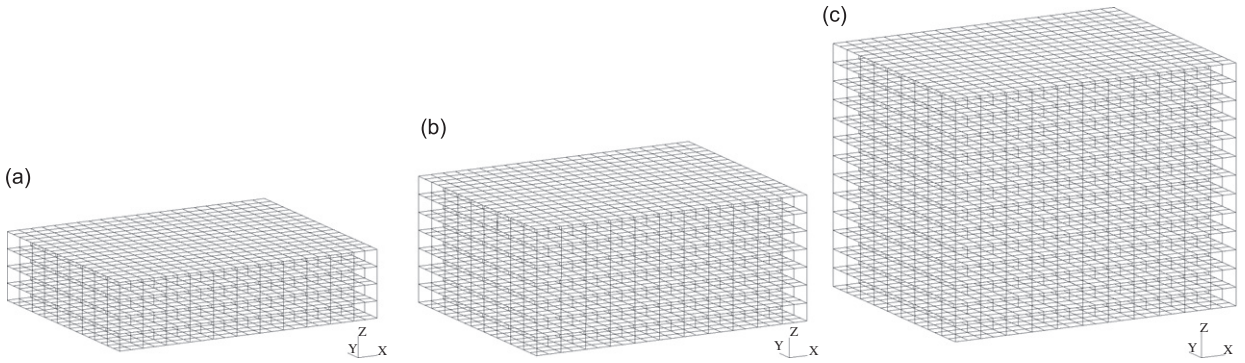

Fig. 7. The three buildings used in the finite element analysis: (a) building case 1, (b) building case 2 and (c) building case 3.

Table 3
Building structure data.

	Building case 1	Building case 2	Building case 3
Stories above ground	3	6	12
Stories under ground	1	1	1
Column size (m)	0.6×0.6	0.8×0.8	0.9×0.9
Beam size (m wide × depth)	0.6×0.4	0.7×0.4	0.8×0.5
Foundation beam size (m)	0.5×1.5	1×2.0	1×3
Slab thickness (m)	0.12	0.12	0.12
Foundation slab thickness (m)	1.5	2.0	3
Depth of retaining wall (m)	10	10	10

and f_l (cycles/m) are the upper and lower limits of the frequency f, respectively, and N is a sufficiently large integer. In this study, the parameters are $N = 1000$, $f_l = 0.01$ cycles/m, $f_u = 3$ cycles/m, and $A = 0.24 \times 10^{-6}$–$40 \times 10^{-6}\,\mathrm{m}^3$/cycle for various numerical analyses.

The location was the Tainan Science Park in southern Taiwan, which contains a soil profile of 10 m inorganic clays of low to medium plasticity, 40 m silty sands, and the rest is very hard sand. The Young's modulus of the surface soil is $0.75\mathrm{E}5\,\mathrm{kN/m}^2$, and that of the soil more than 50 m deep is $8\mathrm{E}5\,\mathrm{kN/m}^2$. Linear interpolation was applied to determine the Young's modulus between these two depths. The mass density and Poisson's ratio of the soil are $2\,\mathrm{T/m}^3$ and 0.48, respectively. The soil shear wave speeds are approximately 250 m/s for the 3 Hz wave. The two factors of Rayleigh damping ([damping] = α[mass] + β[stiffness]) α and β for the soil equal $0.78\,\mathrm{s}^{-1}$ and 3.7×10^{-4} s, respectively, which gives an approximately 2 percent damping ratio at frequencies of 4 and 15 Hz. Shaker experiments were performed to measure the above soil damping using different load frequencies from 2 to 25 Hz, and the least-squares method [24] was used to find α and β by fitting the measured vibration data. An earlier experiment in Ref. [24] concentrated on frequencies from 2 to 25 Hz with a good estimation of the soil damping. This frequency range often generates low-frequency waves within the major part of vehicle-induced vibration.

Three buildings with mat foundations, as shown in Fig. 7 and Table 3, were analyzed. Building case 1 is a three-story factory, case 2 is a six-story building, and case 3 is a 12-story building. They all have the same building plane of 66 m by 54 m with a column spacing of 6 m in both the X and Y axes. The distance between a building and the road edge is 14 m. The story height, both above and underground, is 4 m. A 10 m retaining wall, with a thickness of 0.6 m, was built underground around the building. Column, beam, and slab sizes of the three buildings are listed in Table 3.

The natural frequencies of the three buildings (Table 3) are shown in Table 4. In the natural-frequency analysis, the building mesh was generated in a soil profile with the dimensions of $98 \times 84 \times 52$ m (length × width × depth). Rollers perpendicular to soil profile surfaces were used, except for the upper surface, which had the free boundary condition.

Table 4
Natural frequencies (Hz) of the buildings shown in Table 3.

Building case	Mode	*X* direction	*Y* direction	Rotation-*Z* direction	*Z* direction
1	1	1.87	1.81	1.89	15.00
1	2	6.10	6.08	6.50	16.50
2	1	1.24	1.23	1.35	12.90
2	2	4.01	3.99	4.15	13.20
3	1	0.74	0.73	0.81	7.59
3	2	2.27	2.27	2.34	8.47
3	3	3.99	3.98	4.21	9.92

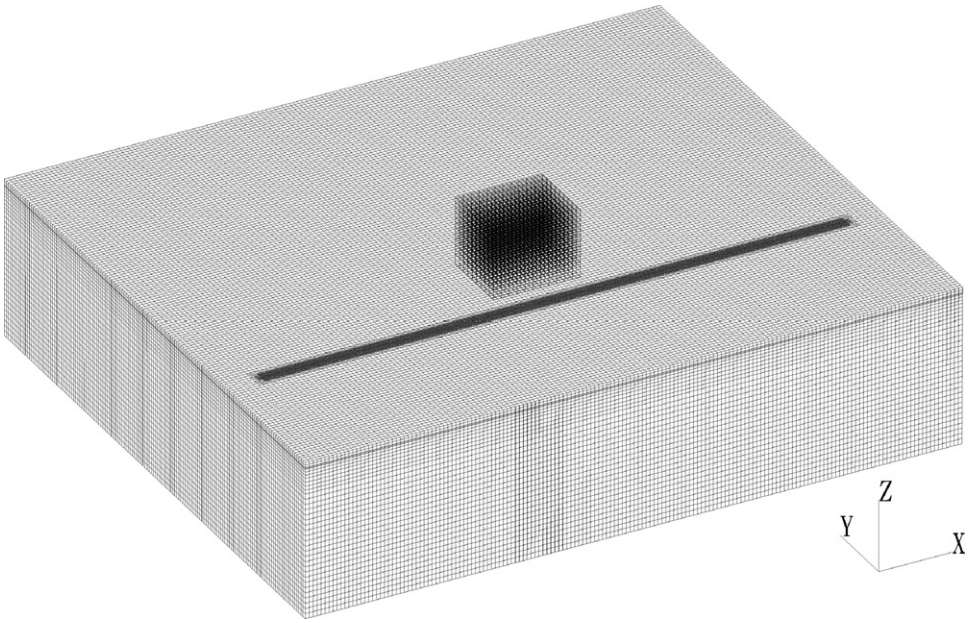

Fig. 8. A typical 3D finite element mesh (1,336,592 nodes).

3.2. Finite element model

The Newmark direct integration method and a consistent mass scheme were used to solve this problem with the solution scheme of the symmetric successive over-relaxation (SSOR) preconditioned conjugated gradient method [25]. The finite element model is 498 m long, 429 m wide, and 120 m deep with a maximum solid element size of 3 m. The soil and road are modeled by 8-node 3D solid elements, the truck is modeled by the moving wheel elements, and the five surfaces, except the top surface of the mesh, are modeled by the absorbing boundary condition [26], which avoids spurious reflections at the boundaries of the soil domain. The nearby building is modeled by 3D beam elements, and its floor slabs and retaining walls are modeled by assumed-strain shell elements. Nodes connected to the 3D beam and shell elements have six dof, three translations, and three rotations. Other nodes have three translation dof Fig. 8 shows a typical 3D finite element mesh, which contains 1,336,592 nodes. The time step length is 0.0135 s, and 2048 time steps were simulated. This time step is about one fifth of the 10 Hz wave period, so it is accurate enough to simulate waves lower than 10 Hz. The soil wavelength for the 10 Hz surface wave approximates to 22 m, which is about seven times the maximum

Table 5
Recommended vibration guidelines.

Description of use	Max. level of vibration (dB)	Description
Workshop	90	Distinctly perceptible vibration. Appropriate for workshops and non-sensitive areas
Office	84	Perceptible vibration. Appropriate for offices and non-sensitive areas
Residential day	78	Barely perceptible vibration. Appropriate for sleeping areas in most instances
Operation room	72	Vibration not perceptible. Adequate in most instance for optical microscopes to 100X
VC-A standard in semi-conductor industries	66	Adequate in most instances for optical microscopes to 400X, microbalances, optical balances, proximity and projection aligners, etc.
VC-D standard in semi-conductor industries	48	Adequate in most instances for optical microscopes (TEM and SEM), microbalances, optical balances, proximity and projection aligners, etc.

element size (3 m), so the finite element analysis should be accurate enough for wave frequencies lower than 10 Hz. However, waves higher than 10 Hz and lower than 30 Hz still contain more than two time steps and two maximum element sizes, so their references should be acceptable.

Analyzing vibrations using the $\frac{1}{3}$ octave band in the frequency domain has become an international standard in semi-conductor industries. Thus, this method, presented in decibels (dB) is utilized in this research. Table 5 briefly presents the recommended vibration guidelines [27]. A frequency-dependent dB and a total dB are used in the subsequent figures, and the calculation procedures can be found in Refs. [27,28].

4. Illustrations and discussions of finite element results

4.1. Comparison of finite element and field experimental results

This section investigates the accuracy of the finite element analysis for the truck-induced vibrations at a free field by comparing the field experiments and finite element analyses. There were two experimental stations at distances of 6 and 30 m from the centerline of the road lane where the truck passed. Each station had a vertical velocity sensor that was set up to measure the vertical vibration velocities. A computer system was used to record the velocity histories of the two stations with a sample rate of 512 Hz (i.e., 512 measurements per second).

The truck, road, and soil are the same as mentioned in Section 3.1, and only the spectral roughness coefficient A is $0.24\times10^{-6}\,m^3$/cycle. The finite element model is the same as that mentioned in Section 3.2, but without the buildings in the finite element mesh. Fig. 9 shows a comparison of the vertical vibration at the two stations between three field measurements and finite element analyses for truck speeds of 30 and 50 km/h. This figure indicates that the accuracy of the model is acceptable. The vibration peak around the frequencies of 2–4 Hz comes from the coincidence of the road irregularity frequencies and the vertical natural frequencies of the truck, which are equal to 2.6 and 3.3 Hz. The vibration peak around the frequencies of 10–20 Hz is caused by the contact forces between the road and truck wheels due to the road irregularity. As a result of the arrangement of the truck mass, springs, and dampers, the vibration will be larger at these frequency ranges.

4.2. Effect of the truck speed

The moving vehicle is the source of vibration, so its speed plays an important role in the vehicle-induced vibration. This section investigates the behavior of the building vibrations generated from an adjacent moving truck with speeds of 20, 30, 40, 50, 70, 90, and 110 km/h. The properties of the truck and soil were mentioned in Section 3.1, where the road center is 14 m from the building edge, and the building analyzed is the third case, as shown in Table 3 and Fig. 7. The road irregularity is classified as very good, as the spectral roughness coefficient (A) is equal to $0.24\times10^{-6}\,m^2/(m/cycle)$ (Table 3). Fig. 10 shows the surface displacements of the finite element analysis for building case 3 under the truck speed of 70 km/h, in which the most obvious wavelength is about 80 m. The major soil wave in the figure is generated from the moving truck around its

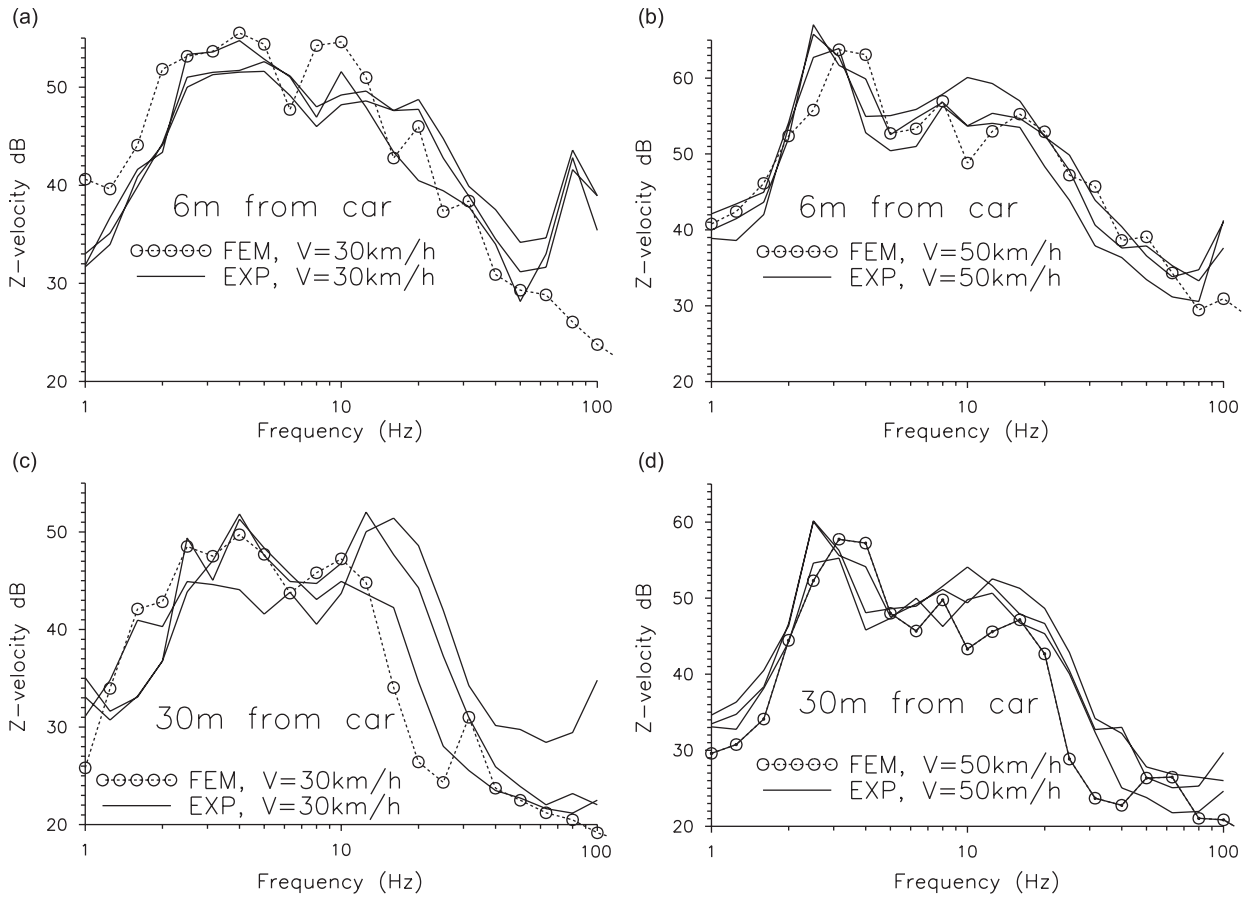

Fig. 9. Comparisons of the vertical vibration at the two stations between three field measurements and the finite element analysis for truck speeds of 30 and 50 km/h: (a) car speed of 30 km/h and 6 m from car, (b) car speed of 50 km/h and 6 m from car, (c) car speed of 30 km/h and 30 m from car and (d) car speed of 50 km/h and 30 m from car.

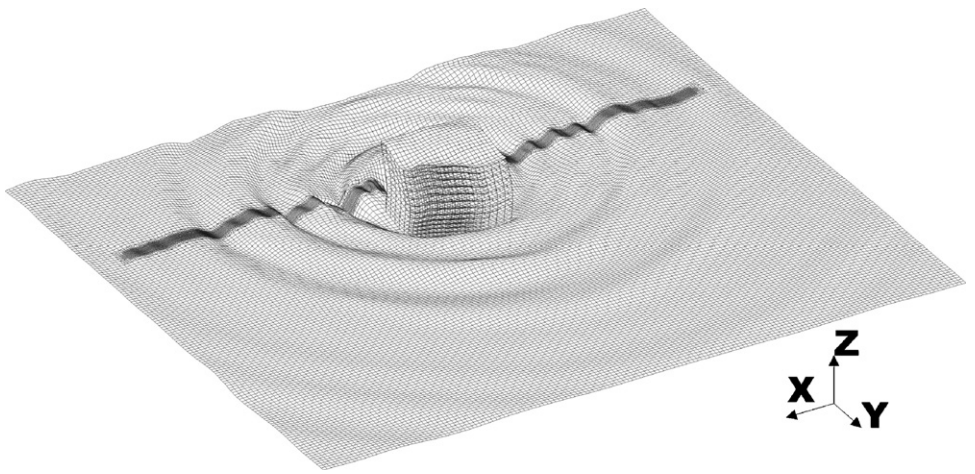

Fig. 10. Surface displacements of a finite element analysis for building case 3 under a truck speed of 70 km/h with the displacement magnifying factor of 3×10^6 (major wavelength is about 80 m).

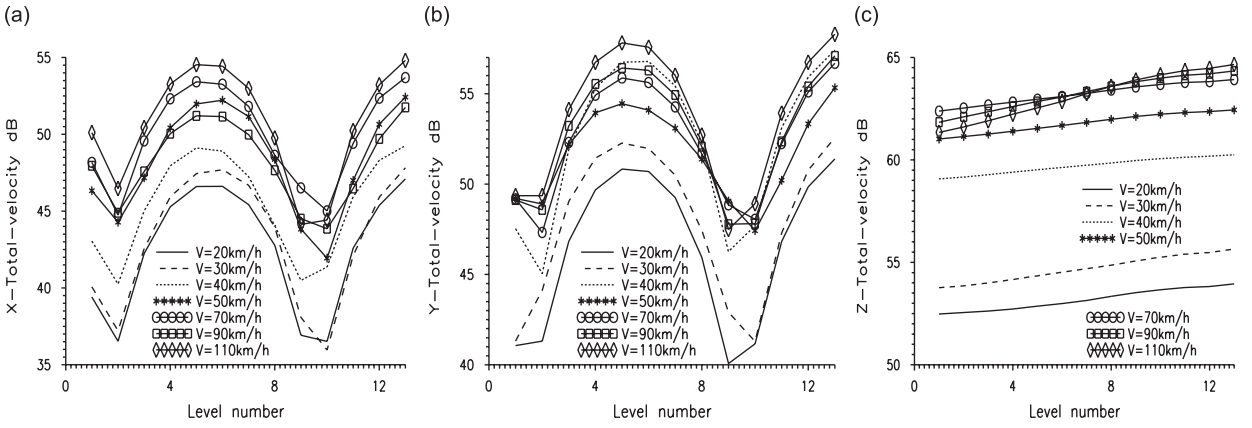

Fig. 11. Particle total velocity dB changing with truck speed for building case 3: (a) X-direction vibration, (b) Y-direction vibration and (c) Z-direction vibration

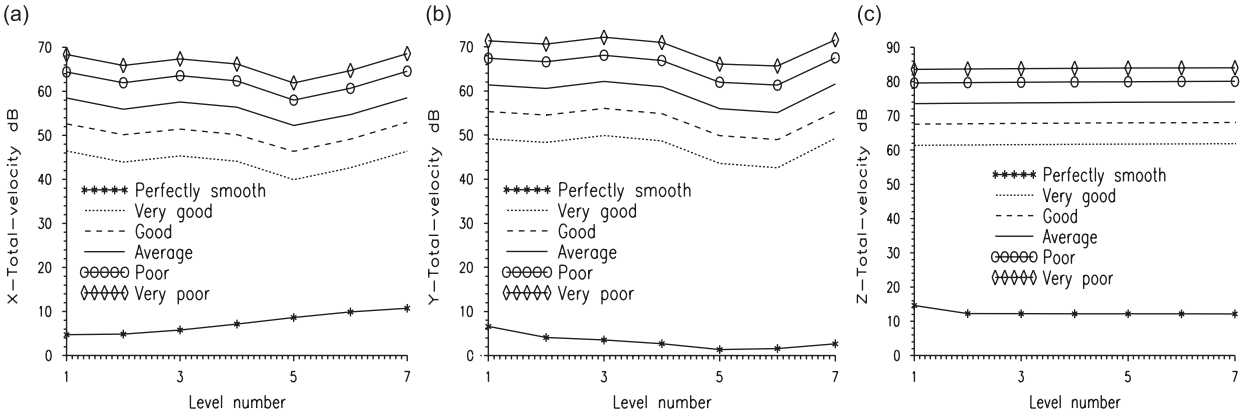

Fig. 12. Particle total velocity dB changing with floor level for building case 2: (a) X-direction vibration, (b) Y-direction vibration and (c) Z-direction vibration.

vertical natural frequencies (2.6 and 3.3 Hz) with the approximate wavelengths of 90 and 70 m. Fig. 11 shows the finite element results, which indicate the following features:

(1) In the Y and Z directions, when the truck speed increases, the building vibrations also increase. This is due to the increase in truck speed producing a larger power spectral density function $G_r(f)$ in Eq. (17) for a certain vibration frequency ($f_{\text{vibration}}$). This vibration frequency ($f_{\text{vibration}}$) is equal to fV, where f is the frequency per unit length in Eq. (17), and V is the truck speed. If the vibration frequency ($f_{\text{vibration}}$) is not changed, a larger V should come with a smaller f, which produces a larger $G_r(f)$ from Eq. (17). Generally, a large power spectral density function causes large vehicle vibrations. The X-direction building vibration is the smallest, which approximately follows this rule.
(2) Fig. 11 shows that the building vibration induced by a fast truck speed appears to have a limit. This is because the power spectral density function in Eq. (17) has a limit for f at 0.05 cycles/m. Moreover, a fast speed has a shorter duration time and may decrease vibrations near the resonance condition.

4.3. Effect of the road irregularity

This section investigates the building vibration induced by the truck due to the effect of the road irregularity. The properties of the truck and soil were mentioned in Section 3.1, where a truck with a speed of

50 km/h moves on a road 14 m from the building edge. The building analyzed is the second case, as shown in Table 3 and Fig. 7. The road irregularity is classified as perfectly smooth, very good, good, average, poor, and very poor as the spectral roughness coefficient (A) equals 0, 0.24×10^{-6}, 1×10^{-6}, 4×10^{-6}, 16×10^{-6}, and $40\times10^{-6}\,m^2/(m/cycle)$, respectively (see Table 3). Fig. 12 shows the maximum total particle velocity dB changing with floor level. This figure indicates that the truck-induced building vibration is extremely small when the road is perfectly smooth. However, with a minor irregularity of the road under a spectral roughness coefficient (A) classified as very good, the truck-induced building vibration is significantly increased, and its value can reach up to 60 dB in the vertical direction. When the road is classified as average, the vertical vibration is larger than 72 dB, which is not suitable for an operating room in a hospital, as shown in Table 5. For this reason, undesirable vibrations of vehicles moving on roads are in large part due to the unevenness of the road surface. The figure also indicates that the vertical building vibration is larger than the in-plane building vibration. This condition represents a truck-induced building vibration in the worst case, because Ju and Lin [29] indicated that a suitable mat foundation can significantly reduce the horizontal vibration transformed from the soil, but cannot reduce vertical low-frequency vibrations. Road irregularity is the most influential factor in producing ground vibrations induced by moving vehicles. Thus, to decrease truck-induced vibrations, the road surface should be as smooth as possible.

4.4. *Effect of building structures*

This section studies truck-induced vibrations due to the effect of building structures. Shear walls and thicker floor slabs can increase the building stiffness, so they are often used to reduce building vibrations. Thus, finite element analyses were performed for the three building (Table 3) with a truck speed of 50 km/h and the conditions of (1) 35 cm-thick shear walls constructed around the building (shear-wall case), and (2) the thickness of all 12 cm floor slabs replaced by 100 cm ones (thick-slab case). Fig. 13 shows the particle frequency-dependent velocity dB in the Y and Z directions at the roof, and Fig. 14 shows the maximum total particle velocity dB changing with floor levels. The two figures indicate the following features:

(1) Fig. 13 shows that the Y- and Z-direction vibrations are concentrated at the frequencies between 2 and 5 Hz, which is caused by the truck vibrating at its vertical natural frequencies (2.6 and 3.3 Hz) (see Fig. 10). Because the building foundation slab can reduce high-frequency vibrations [29], the vibrations with

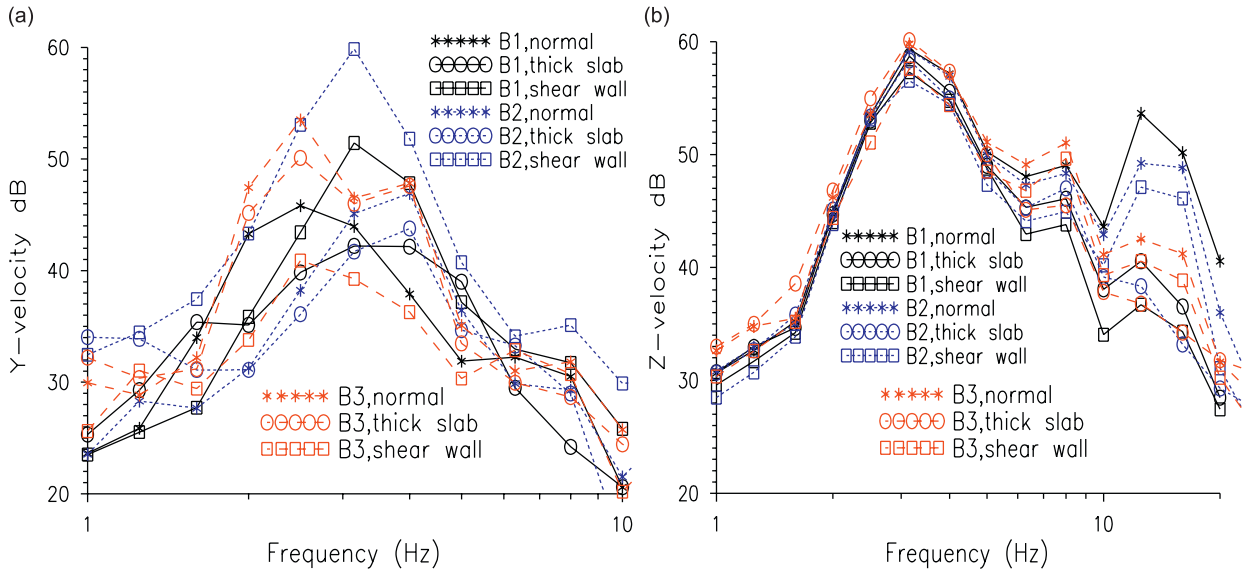

Fig. 13. Particle frequency-dependent velocity dB for the three building cases (truck speed = 50 km/h): (a) Y-direction vibration and (b) Z-direction vibration.

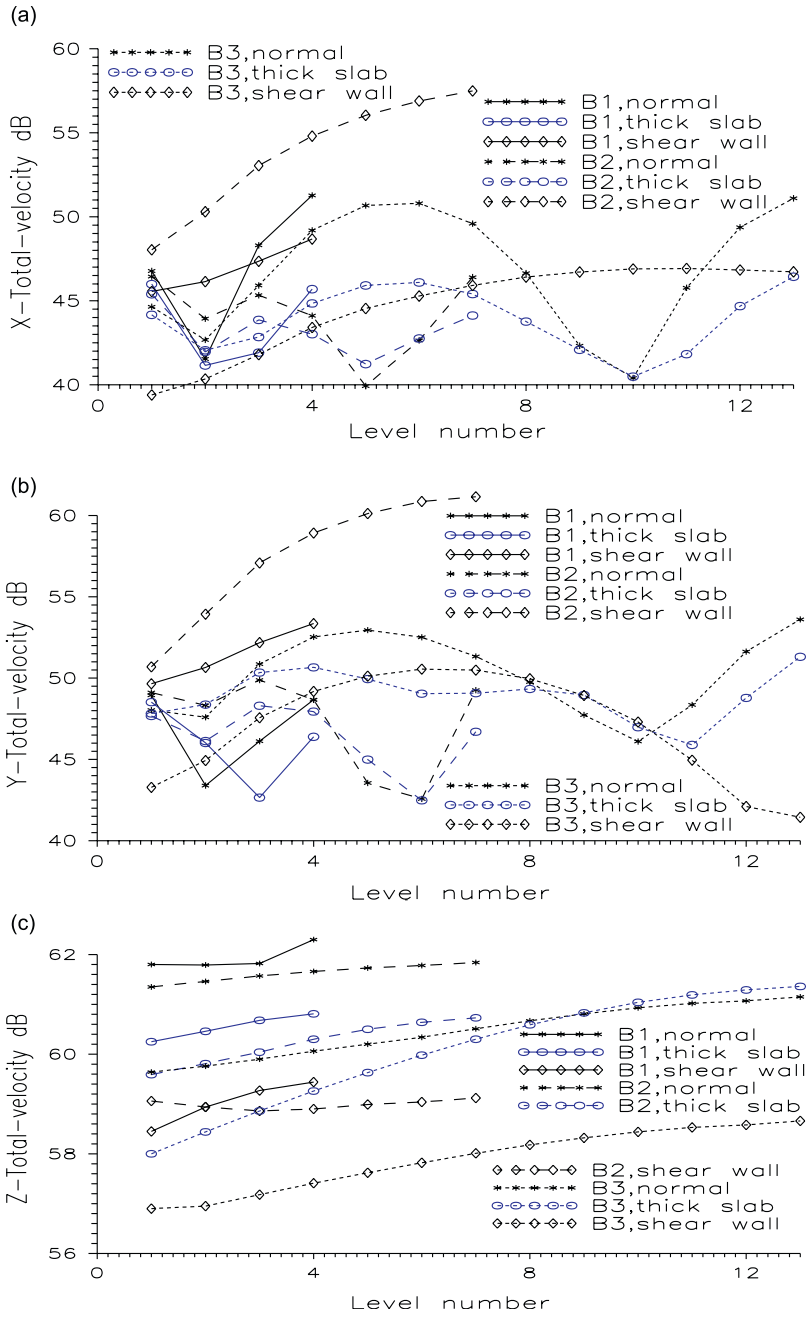

Fig. 14. Particle total velocity dB changing with floor level for the three building cases (truck speed = 50 km/h): (a) X-direction vibration, (b) Y-direction vibration and (c) Z-direction vibration.

frequencies higher than 10 Hz in the Y-direction and 20 Hz in the Z-direction are relatively small, so they are not shown in the figure. The peaks of Z-direction vibrations between 7 and 20 Hz are due to the first vertical natural frequency of buildings. This figure further indicates that truck vertical natural frequencies play an import role in vehicle-induced vibration.

(2) For the in-plane (X- and Y-directions) vibrations of building case 1, the thick-slab case has the smallest vibrations, and the shear-wall case has the largest. This is because the first and second in-plane natural frequencies of the thick-slab case are 1.5 and 5.4 Hz, respectively, which is very different from the truck's

vertical frequencies of 2.6 and 3.3 Hz. However, the first in-plane natural frequency of the shear-wall case is 2.9 Hz, which is close to the first vertical natural frequency of the truck, so resonance causes a large vibration of the shear-wall building and demonstrates a first-mode vibration pattern, as shown in Fig. 14.

(3) For the in-plane vibrations of building case 2, the normal and thick-slab cases have smaller vibrations, and the shear-wall case has the largest. The reason is similar to the above discussed; the first and second in-plane natural frequencies of the thick-slab case are very different from the truck's vertical frequencies, but the first in-plane natural frequency of the shear-wall case is 2.5 Hz, which is very close to the first vertical natural frequency of the truck, so resonance causes the building vibration to be the largest and also demonstrates a first-mode vibration pattern, as shown in Fig. 14.

(4) For the in-plane vibrations of building case 3, Fig. 14 shows that the normal case has the largest vibrations. This is because the second and third in-plane natural frequencies (2.27 and 3.99 Hz) of the normal case are near the truck vertical frequencies (2.6 and 3.3 Hz), which causes the building vibrations to be large and demonstrates a third-mode vibration pattern, as shown in Fig. 14. The shear-wall case increases the first and second in-plane natural frequencies to 1.5 and 4.2 Hz, which are considerably different from the truck's vertical natural frequencies, so the building vibration is small.

(5) For the vertical vibrations, the natural frequencies of all the building cases are much larger than the truck's natural frequencies, so resonance is not evoked, and the building stiffness can decrease the vibration. Fig. 14 shows that the shear-wall building has the best performance. The thick-slab building can also decrease the vertical vibration, but the efficiency is not high compared to its cost. Moreover, the large mass of thick slabs may decrease the building's vertical natural frequencies. If they approach the truck's natural frequencies, the vertical building vibrations will be increased. This condition can be found in Fig. 14 for building case 3 with thick slabs. However, because of the large difference between the truck and building vertical natural frequencies, the vibration difference between the three building types is about only 2–4 dB.

(6) The above discussions indicate a simple fact: the vertical natural frequencies of the truck are the most critical factor that influences the building vibration. Road irregularities evoke the truck's vibrations around its vertical natural frequencies. If these frequencies approach the building natural frequencies, resonance occurs and the building vibrations are large. Moreover, the shape of the building vibration is similar to the mode shape of the resonance building frequency. Generally, the resonance at the first building natural frequency is the most serious. Although Ju and Lin [28] also indicated a similar resonance phenomenon for train-induced vibration, the source of the vehicle and train frequencies is different. For trains, the dominant frequencies come from the periodic wheel loads, while for vehicles the natural frequencies are the most important element. To reduce building vibrations generated from adjacent moving trucks, the road roughness should be as small as possible and the truck vibration at its vertical natural frequency should be decreased. A simple scheme to reduce truck vibrations is to slow down the truck speed.

5. Conclusions

This study developed a finite element method to simulate complicated 3D vehicles moving on a road, where car bodies, bogies, wheel-axis sets, springs, and dampers are modeled by assembling moving wheel elements, spring-damper elements, lumped masses, and rigid links. The theory and formulations of this vehicle model are simple and can be added to standard dynamic finite element codes without difficulty. Fryba's solution of a simply supported beam subjected to a moving two-axle system was analyzed to validate this finite element model. The simulations, including road irregularities and changing the mesh of solid elements, are almost identical for the two schemes, which means that the proposed finite element model of moving vehicles is considerably accurate. Field experiments were also used to validate the current model, and a comparison between field experiments and finite element analyses also indicates that the current model has acceptable accuracy.

This paper indicates that road irregularity is the major source of truck vibrations around its vertical natural frequencies, which play an important role in field and building vibrations. If these frequencies approach the building's natural frequencies, resonance occurs, which causes large building vibrations. Furthermore, the

shape of the building vibration is similar to the mode shape of the resonance building frequency. The numerical results indicate that the resonance at the first building natural frequency is the most serious, even when shear walls or thick slabs are used to reinforce the building. To reduce building vibrations generated from adjacent moving trucks, the road roughness should be as small as possible, and the truck's vibrations at its vertical natural frequency should be decreased. More readily, truck vibrations can be reduced by slowing down the truck speed. Moreover, the coincidence of the first building natural frequency and the truck vertical natural frequency should be avoided. If this type of resonance does not occur, the shear-wall building has the best performance in decreasing building vibrations.

References

[1] O. Hunaidi, M. Tremblay, Traffic-induced building vibrations in Montreal, *Canadian Journal of Civil Engineering* 24 (5) (1997) 736–753.
[2] S. Maeda, M. Morioka, Y. Yonekawa, et al., Experimental studies of subjective response to road traffic-induced building vibration, *Industrial Health* 36 (2) (1998) 112–119.
[3] P. Clemente, D. Rinaldis, Protection of a monumental building against traffic-induced vibrations, *Soil Dynamics and Earthquake Engineering* 17 (5) (1998) 289–296.
[4] H. Hao, T.C. Ang, Analytical modeling of traffic-induced ground vibrations, *Journal of Engineering Mechanics—ASCE* 124 (8) (1998) 921–928.
[5] H. Hao, T.C. Ang, J. Shen, Building vibration to traffic-induced ground motion, *Soil Dynamics and Earthquake Engineering* 19 (7) (2000) 473–488.
[6] G. Lombaert, G. Degrande, D. Clouteau, Numerical modelling of free field traffic-induced vibrations, *Soil Dynamics and Earthquake Engineering* 19 (7) (2000) 473–488.
[7] O. Hunaidi, W. Guan, J. Nicks, Building vibrations and dynamic pavement loads induced by transit buses, *Soil Dynamics and Earthquake Engineering* 19 (6) (2000) 435–453.
[8] G. Lombaert, G. Degrande, Experimental validation of a numerical prediction model for free field traffic induced vibrations by in situ experiments, *Soil Dynamics and Earthquake Engineering* 21 (6) (2001) 485–497.
[9] M. Crispino, M. D'apuzzo, Measurement and prediction of traffic-induced vibrations in a heritage building, *Journal of Sound and Vibration* 246 (2) (2001) 319–335.
[10] G. Lombaert, G. Degrande, D. Clouteau, The influence of the soil stratification on free field traffic-induced vibrations, *Archive of Applied Mechanics* 71 (10) (2001) 661–678.
[11] D. Clouteau, G. Degrande, G. Lombaert, Numerical modelling of traffic induced vibrations, *Meccanica* 36 (4) (2001) 401–420.
[12] M. Schevenels, G. Degrande, G. Lombaert, The influence of the depth of the ground water table on free field road traffic-induced vibrations, *International Journal for Numerical and Analytical Methods in Geomechanics* 28 (5) (2004) 395–419.
[13] L. Pyl, G. Degrande, G. Lombaert, W. Haegeman, Validation of a source-receiver model for road traffic-induced vibrations in buildings. I: Source model, *Journal of Engineering Mechanics—ASCE* 130 (12) (2004) 1377–1393.
[14] Y.L. Xu, X.J. Hong. Stochastic modelling of traffic-induced building vibration, *Journal of Sound and Vibration* 313 (1–2) (2008) 149–170.
[15] S.H. Ju, H.T. Lin, C.C. Hsueh, S.L. Wang, A simple finite element model for vibration analyses induced by moving vehicles, *International Journal for Numerical Method in Engineering* 68 (2006) 1232–1256.
[16] K.J. Bathe, *Finite Element Procedures*, Prentice-Hall International, Engelwood Cliffs, NJ, 1996.
[17] S.H. Ju, H.T. Lin, Investigating vehicle dynamic response due to braking and acceleration, *Journal of Sound and Vibration* 303 (1–2) (2007) 46–57.
[18] S.H. Ju, Three-dimensional analyses of wave barriers for reduction of train-induced vibrations, *Journal of Geotechnical and Geoenvironmental Engineering* 130 (7) (2004) 740–748.
[19] S.H. Ju, H.T. Lin, Experimentally investigating finite element accuracy for ground vibrations induced by high-speed trains, *Engineering Structures* 30 (3) (2007) 733–746.
[20] L. Fryba, *Vibration of Solids and Structures under Moving Load*, Thomas Telford, London, 1999.
[21] F.T.K. Au, Y.S. Cheng, Y.K. Cheung, Effects of random road surface roughness and long-term defection of prestressed concrete girder and cable-stayed bridges on impact due to moving vehicles, *Computers and Structures* 79 (2001) 853–872.
[22] M. Shinozuka, C. Jan, Digital simulation of random processes and its application, *Journal of Sound and Vibration* 25 (1972) 111–128.
[23] M. Shinozuka, G. Deodatis, Simulation of stochastic processes by spectral representation, *Applied Mechanics Reviews* 44 (1991) 191–204.
[24] S.H. Ju, S.H. Ni, Determining Rayleigh damping parameters of soils for finite element analysis, *International Journal for Numerical and Analytical Methods in Geomechanics* 31 (10) (2007) 1239–1255.
[25] S.H. Ju, K.S. Kung, Mass types, element orders and solving schemes for the Richards equation, *Computers & Geosciences* 23 (1997) 175–187.
[26] S.H. Ju, Y.M. Wang, Time-dependent absorbing boundary conditions for elastic wave propagation, *International Journal for Numerical Method in Engineering* 50 (2001) 2159–2174.

[27] C.G. 1991 Gordon SPIE1619, 71-75. Generic criteria for vibration sensitive equipment.
[28] S.H. Ju, Finite element analysis of structure-borne vibration from high-speed train, *Soil Dynamics and Earthquake Engineering* 27 (3) (2007) 259–273.
[29] S.H. Ju, H.T. Lin, Reduction of vibrations due to foundation slabs, *Journal of Geotechnical and Geoenvironmental Engineering, ASCE* 132 (4) (2006) 511–520.